


RESEARCH LETTER

Glu592 of the axon guidance receptor ROBO3 mediates a pH-dependent interaction with NELL2 ligand

Kimihiko Mizutani¹, Mayuko Toyoda¹, Teruyo Ojima-Kato², Andrés D. Maturana² and Tomoaki Niimi² 

¹ Graduate School of Agriculture, Kyoto University, Japan

² Graduate School of Bioagricultural Sciences, Nagoya University, Japan

Correspondence

T. Niimi, Graduate School of Bioagricultural Sciences, Nagoya University, Furo-cho, Chikusa-ku, Nagoya 464-8601, Japan
 Tel: +81 52 789 5015
 E-mail: tmiimi@agr.nagoya-u.ac.jp

(Received 26 August 2024, revised 9 October 2024, accepted 21 October 2024)

doi:10.1002/1873-3468.15054

Edited by Hee-Jung Choi

There are only a few studies on the function of neuronal axon guidance molecules during low brain pH conditions. We previously reported that roundabout (ROBO) 2, a receptor for the axon guidance molecule SLIT, can bind to the neural epidermal growth factor-like-like (NELL) ligands in acidic conditions by conformational change of its ectodomain. Here, we show that the ROBO3 receptor also exhibits a pH-dependent increase in binding to the NELL2 ligand. We found that the Glu592 residue of ROBO3 at the binding interface between NELL2 and ROBO3 is a pH sensor and that the formation of a new hydrogen bonding network, due to protonation of the Glu592, leads to increased binding in acidic conditions. These results suggest that NELL2–ROBO3 signaling could be regulated by extracellular pH.

Keywords: axon guidance; extracellular pH; protein conformation; protein–protein interaction; structural model

Typically, under homeostatic conditions, brain pH in healthy individuals is strictly regulated. However, neural activity can induce temporary and local pH fluctuations in which acid-sensitive ion channels detect a decrease in extracellular pH and induce neuronal responses and signaling in the stress environment [1,2]. In pathological conditions such as epilepsy and cerebral ischemia, neuronal damage and abnormal brain activity have been observed alongside changes in extracellular pH, indicating a link between pH changes and the pathology [3,4]. Postmortem analyses of patients with schizophrenia or bipolar disorder have shown below-average brain pH in these conditions [5–8]. This decrease in brain pH is theorized to be related to increased lactate levels due to abnormal energy metabolism, but the exact cause is unknown, and the functional significance of brain acidity in neuropsychiatric disorders is unclear [7,9,10]. As described above, changes in brain pH are thought to

affect various biological processes, including gene expression in the brain [11], but the physiological significance of brain pH changes remains unresolved.

During nervous system development, axon guidance is a critical process for correct neuronal circuit formation and involves a diverse group of molecules [12–15]. SLIT–Roundabout (ROBO) signaling, which is transduced by the binding of SLIT ligands to ROBO receptors, is known to regulate commissural projection pathways in the central nervous system, as well as cell–cell interactions outside the nervous system [16–19]. SLIT–ROBO signaling has been reported to promote neuronal migration and regeneration when the brain is damaged [20], and mutations in the SLIT–ROBO family of genes have been reported in various neurological and psychiatric disorders [21–25].

Although ROBO1 and ROBO2 are known receptors for SLIT ligands, Jaworski *et al.* [26] reported that

Abbreviations

ECD, ectodomain; EGFL, epidermal growth factor-like; FNIII, fibronectin type III; Ig, immunoglobulin-like; NELL, neural epidermal growth factor-like (NEL)-like; ROBO, roundabout.

neural epidermal growth factor-like-like (NELL) 2, a member of the NELL family proteins, negatively regulates SLIT–ROBO signaling in axon guidance by binding to the ROBO3 receptor, the ligand for which was previously unknown. We previously reported that the NELL ligands cannot bind to the ROBO2 receptor in neutral conditions, but can do so in acidic conditions [27]. The binding sites of the NELL ligand and the ROBO receptor are the epidermal growth factor-like (EGFL) 2–3 and fibronectin type III (FNIII) 1 domains, respectively. However, in neutral conditions, the FNIII1 domain is masked by the immunoglobulin-like (Ig) 5 domain because of the hairpin-like structure of the ectodomain (ECD) of ROBO2 [27,28]. In acidic conditions, conformational changes in the hairpin-like structure expose the FNIII1 domain, allowing access to the NELL ligand [27,29]. When we analyzed the interaction between NELL ligands and ROBO receptors under different pH conditions, we found that the interaction between NELL ligands and ROBO3 also increased in acidic conditions, but the mechanism of the increase was unclear [27]. Subsequently, the crystal structure of the NELL2–ROBO3 complex was reported by Pak *et al.* [30], who found that the ectodomain of ROBO3 takes an extended open structure rather than a hairpin-like structure. This suggests that the increase in NELL ligand–ROBO3 binding in acidic conditions is due to a different mechanism than conformational changes in hairpin-like structures such as ROBO2 [27,29].

In this study, we show that the interaction between NELL2 and ROBO3 increases in a pH-dependent manner using various experimental systems. We identified Glu592 of ROBO3 as an amino acid residue present at the NELL2–ROBO3 binding interface that changes the protonation state in an acidic pH range. The Glu592 residue was protonated in acidic conditions, presumably to form hydrogen bonds with Asp476 of NELL2, thereby increasing binding affinity. Mutation analysis showed that replacing the Glu592 residue with Gln592 abolished the increase in binding in acidic conditions. These results suggest that the Glu592 residue acts as a pH sensor for a pH-dependent interaction between NELL2 and ROBO3 and that NELL2–ROBO3 signaling is regulated by extracellular pH.

Materials and methods

Antibodies

Mouse monoclonal antibodies against FLAG (Sigma-Aldrich, St. Louis, MO, USA), hemagglutinin (HA) (MBL,

Nagoya, Japan), c-Myc (MBL), and His (MBL) epitopes were purchased from the indicated manufacturers. Horseradish peroxidase (HRP)–conjugated anti-mouse and anti-human IgGs were purchased from Cytiva (Tokyo, Japan) and Proteintech (Rosemont, IL, USA), respectively.

Plasmid construction

An expression vector for human ROBO3 ectodomain with a C-terminal human immunoglobulin Fc-tag (ROBO3-ECD-Fc) was prepared as follows: a cDNA encoding the human ROBO3 (residues 21–891) was amplified by RT-PCR from total RNA isolated from human brain (Invitrogen, Carlsbad, CA, USA). This cDNA contains a micro-exon 6b sequences (e6b+) [29]. The PCR product was digested with appropriate restriction enzymes, cloned into the pSecTag2A-Fc vector, which was generated by subcloning a cDNA encoding the Fc fragment into the *XhoI*–*ApaI* sites of the pSecTag2A mammalian expression vector (Invitrogen). An expression vector for three FNIII domains of human ROBO3 (residues 555–891) with a C-terminal Fc-tag (ROBO3-FNIII-Fc) was generated by subcloning a PCR fragment from a ROBO3-ECD-Fc plasmid into the *EcoRI*–*XhoI* sites of pSecTag2A-Fc vector. The single amino acid substitution mutants (E592A, E592Q, and R630A) were generated by inverse PCR-based site-directed mutagenesis using a KOD-plus DNA polymerase (Toyobo, Osaka, Japan). An expression vector for human ROBO3 ectodomain with an N-terminal HA-tag (HA-ROBO3-ECD) was prepared similarly except that the PCR product was cloned into the pSecTag2A-HA vector [27]. An expression vector for full-length mouse Robo3 (Robo3-FL; residues 1–1402) were prepared as described previously [27].

An expression vector for full-length human NELL2 with an N-terminal alkaline phosphatase (AP)-tag (AP-NELL2-FL) was prepared as described previously [27]. The single amino acid substitution mutants (D476A, H449A, H483A, H491A, and H506A) were generated by inverse PCR-based site-directed mutagenesis. An expression vector for the N-terminal FLAG-tagged mouse Nell2 lacking its C-terminal region (FLAG-Nell2-ΔC; residues 25–525) was generated by inverse PCR-based deletion from a full-length mouse Nell2 expression vector [27]. We expressed and purified a soluble mouse Nell2 protein lacking its C-terminal region that is dispensable for binding to ROBO3, because the full-length mouse and human NELL2 expression vectors with relatively small tags are either not secreted or have very low expression efficiency.

Protein expression and purification

Recombinant NELL2 and ROBO3 proteins were produced by the FreeStyle MAX 293 Expression System (Invitrogen), according to the manufacturer's instructions (Fig. S1). Briefly, FreeStyle 293-F human embryonic kidney cells

(RRID: CVCL_D603) were transfected with the expression plasmids using the FreeStyle MAX Reagent (Invitrogen) and grown in serum-free FreeStyle 293 Expression medium (Invitrogen) for 2–5 days. When necessary, recombinant proteins with hexahistidine tag were purified from the conditioned media using Ni Sepharose 6 Fast Flow (Cytiva) or 1-mL His60 Ni Superflow Cartridge (Clontech, Mountain View, CA, USA). Purified proteins were analyzed by sodium dodecyl sulfate–polyacrylamide gel electrophoresis (SDS/PAGE) under reducing conditions, and separated proteins were visualized by silver staining (EzStain Silver, Atto, Tokyo, Japan) or Coomassie Brilliant Blue (CBB) R-250 staining (Quick-CBB, Wako, Osaka, Japan).

Immunoblot analysis

Proteins were separated on SDS-polyacrylamide gels, followed by transfer onto Amersham Protran Premium 0.45 nitrocellulose membranes (Cytiva). The membranes were blocked with 5% (w/v) skim milk in phosphate-buffered saline (PBS) containing 0.1% (v/v) Tween 20, followed by incubation with the primary antibody for 1 h at room temperature. The membranes were then washed and incubated with the HRP-conjugated secondary antibody for 1 h at room temperature. The membranes were developed with the ECL start Western Blotting Detection Reagent (Cytiva) and imaged on an LAS-4000mini Luminescent Image Analyzer (Cytiva).

Cell-free binding assay

Solid-phase binding assays were performed using Pierce Protein A-coated plates (Thermo Scientific, Waltham, MA, USA). Wells were blocked with HBAH buffer [0.2% (w/v) bovine serum albumin (BSA) and 20 mM HEPES, pH 7.0 in Hank's balanced salt solution] for 15 min. Fc-tagged proteins were allowed to bind to wells for 1 h at room temperature. Wells were washed three times with HBAH buffer, treated with AP-tagged proteins for 1 h at room temperature and then washed three times with HBAH buffer. When analyzed under various pH conditions, AP-tagged proteins were diluted in 50 mM HEPES (pH 7.4, 7.0, and 6.8) or 50 mM MES (pH 6.5) buffer containing 150 mM NaCl. The bound AP activity (absorbance at 590 nm per time) was measured using the KPL BluePhos Microwell Phosphatase Substrate System (SeraCare, Milford, MA, USA).

Solution binding assays were performed as follows: Conditioned media containing HA-ROBO3-ECD and FLAG-Nell2-ΔC were mixed and diluted in 50 mM HEPES (pH 7.4, 7.0, and 6.8) or 50 mM MES (pH 6.5) buffer, and incubated at 4 °C for 1 h. The complex was immunoprecipitated with anti-FLAG M2 affinity beads (Sigma-Aldrich) at 4 °C for 1 h. The beads were washed three times with

HEPES or MES buffer, and the complex was eluted with 150 μg·mL⁻¹ FLAG peptide (Sigma-Aldrich). The eluted samples were separated on SDS-polyacrylamide gels and immunoblotted with the anti-HA and anti-FLAG antibodies.

Cell surface binding assay

Monkey kidney COS-1 cells were maintained in Dulbecco's modified Eagle's medium (DMEM) containing 10% (v/v) fetal calf serum (FCS). Transient transfection of full-length mouse Robo3 expression vector in COS-1 cells was carried out using the FuGENE HD Transfection Reagent (Promega, Madison, WI, USA), according to the manufacturer's instructions. The conditioned media containing AP-NELL2-FL were diluted in 50 mM HEPES (pH 7.4) or 50 mM MES (pH 6.5) buffer containing 150 mM NaCl and then incubated with transiently transfected COS-1 cells for 90 min at room temperature. Cells were washed three times with HEPES or MES buffer and fixed in 4% (w/v) paraformaldehyde for 15 min. Fixed cells were washed three times with 20 mM HEPES (pH 7.0)/150 mM NaCl, incubated at 65 °C for 100 min to inactivate endogenous AP, washed with AP buffer (100 mM Tris/HCl, pH 9.0, 150 mM NaCl, 1 mM MgCl₂) and stained with the 5-bromo-4-chloro-3-indolyl-phosphate (BCIP)-nitroblue tetrazolium (NBT) Solution Kit (Nacalai Tesque, Kyoto, Japan) at 37 °C.

Biolayer interferometry (BLI) analysis

The binding properties of NELL2 and ROBO3 were analyzed by biolayer interferometry by using BLItz system (Sartorius, Goettingen, Germany). The purified ROBO3-ECD-Fc protein was biotinylated using Biotin Labeling Kit-NH2 (Dojindo Molecular Technologies, Kumamoto, Japan) and immobilized on a streptavidin sensor for 120 s in WS buffer (Dojindo Molecular Technologies). Subsequently, we measured the association (120 s) of purified FLAG-Nell2-ΔC at various concentrations in 10 mM HEPES (pH 7.4) or 10 mM MES (pH 6.5) buffer containing 150 mM NaCl, 0.01% (w/v) BSA, and 0.002% (v/v) Tween 20, and their dissociation (120 s) in respective buffers in order to determine the K_D by using a global fitting mode in a 1:1 binding model (BLITZ PRO SOFTWARE, version 1.2.1.3, Sartorius).

Molecular modeling

The crystal structure of the human NELL2–ROBO3 complex was obtained from the Protein Data Bank (PDB ID: 6POG). Protonation states at each pH were assigned using the PROTONATE 3D tool in Molecular Operating Environment (MOE) software package (version 2022.02; Chemical Computing Group, Montreal, QC, Canada). Subsequently,

energy minimization calculations for protonated structures of NELL2–ROBO3 complex were performed using MOE with Amber10:EHT force field. Finally, the intra- and intermolecular hydrogen bonds network was analyzed at pH 7.4 and 6.0. The generated models were saved as pdb files and then imported into the program UCSF CHIMERA version 1.14 for visualization [31].

Results and Discussion

Acidic pH increases the affinity between NELL2 and ROBO3

The interaction between NELL2 and ROBO3 at neutral to acidic pH range was analyzed using various experimental systems and epitope-tagged constructs (Fig. 1A). In solid-phase binding assays, no binding of AP-tagged NELL2 was observed with the Fc protein alone. However, when a fusion protein with the ECD of ROBO3 was used, the binding activity of AP-tagged NELL2 increased as the pH was decreased from 7.4 to 6.5 (Fig. 1B). Similarly, the binding activity of AP-tagged NELL2 increased with decreasing pH when using a region consisting of only three FNIII domains (FNIII) of ROBO3. The binding activity of the ROBO3-FNIII was approximately three-fold higher than that of the ROBO3-ECD, suggesting that the Ig domains of ROBO3 can also be a steric hindrance to NELL2 binding. ROBO3-ECD also exhibited a concentration-dependent increase in NELL2 binding activity at pH 6.5 but not at pH 7.4 (Fig. 1C). Next, we performed binding assays in solution using FLAG-tagged mouse Nell2-ΔC and HA-tagged ROBO3-ECD. As shown in Fig. 1D, co-immunoprecipitation with anti-FLAG antibody showed that the highest amount of ROBO3-ECD was observed at pH 6.5. To investigate whether NELL2 interacts with membrane-bound ROBO3, COS-1 cells were transiently transfected with the full-length mouse Robo3-expressing plasmid. The cells were incubated with AP-tagged NELL2, and bound NELL2 was assessed by *in situ* staining. Consistent with the results of the cell-free binding assays, AP-tagged NELL2 showed strong staining of cells expressing Robo3 at pH 6.5 (Fig. 1E). Unlike in previous reports, NELL2–ROBO3 binding was barely observed at neutral pH in these assays, which was due to the low sensitivity of the assays to suppress the background signals. If the assay conditions were changed (e.g., by increasing the concentration of NELL2), NELL2–ROBO3 binding could be observed at neutral pH. Finally, we confirmed the interaction between Nell2-ΔC and ROBO3-ECD under different pH values (7.4 and 6.5) using biolayer interferometry analysis

(Fig. 1F, Table S1). The equilibrium K_D values were 831 ± 67 nM at pH 7.4 and 3.10 ± 1.83 nM at pH 6.5 (means \pm SD of three replicates). These results indicated that the affinity between NELL2 and ROBO3 is strongly increased at an acidic pH.

Structural differences of the NELL2–ROBO3 complex at neutral and acidic pH

The increase in the binding affinity between NELL2 and ROBO3 at an acidic pH also occurs with ROBO3-FNIII. Therefore, it is considered that the increase is not due to the conformational changes as seen in the hairpin-like structure of ROBO2-ECD but is directly affected by the protonation state of charged amino acids located at the NELL2–ROBO3 binding interface. Histidine residues, with an approximate pK_a of 6.5 (Table 1) [32], are often responsible for pH-dependent changes in binding state when located at the binding interface. There are no conserved histidine residues in the FNIII1 domain of ROBO3, but four conserved histidine residues (His449, His483, His491, and His506) in the EGFL2 and EGFL3 domains of NELL2 (Fig. S2A). Of these, only the His449 residue is located at the NELL2–ROBO3 binding interface. However, when amino acid substitution mutants were created and examined in solid-phase binding assays, there was no significant change in pH-dependent NELL2–ROBO3 binding in either histidine mutant (Fig. S2B). Therefore, we predicted the pK_a values of the charged amino acids located at the binding interface from the NELL2–ROBO3 complex structure with an energy-minimized calculation considering the protonation state at neutral and acidic pH using the MOE software. We found that, from neutral to acidic pH, the Glu592 residue of ROBO3 had a significant shift in its pK_a value from the model- pK_a (Table 1) [32]. The pK_a of the Glu592 residue is predicted to be 6.8 at pH 7.0, so the carboxyl group of the side chain is deprotonated at a neutral pH, but most of them are protonated around pH 6.5. Therefore, structural models of the NELL2–ROBO3 complex at pH 7.4 and pH 6.0 were created using MOE software (Fig. 2). At pH 7.4, a salt bridge likely forms between Asp476 and Arg630, but the side chains of Asp476 and Glu592 are electrostatically repulsive because both have a negative charge. Conversely, at pH 6.0, the carboxyl group of the side chain of Glu592 was protonated, and an additional hydrogen bond between Asp476 and Glu592 is formed. Furthermore, because the pK_a of Glu592 is predicted to be 10.5 at pH 6.0 (Table 1), the carboxyl group of the side chain is fully protonated and the hydrogen bond between Asp476

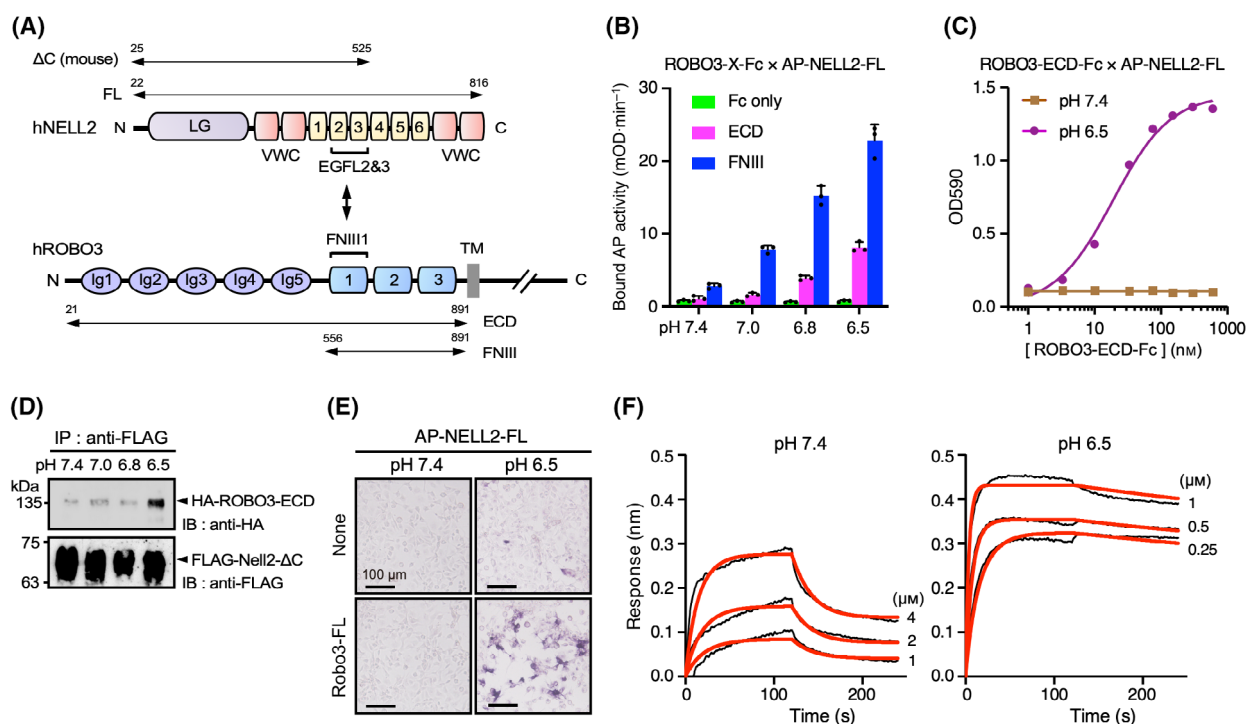


Fig. 1. pH-dependent interaction between NELL2 and ROBO3. (A) Schematic diagrams of structural domains and constructs of human NELL2 and ROBO3. The second and third EGFL domains of NELL2 bind to the FNIII1 domain of ROBO3. The numbers above double arrows indicate amino acid position. EGFL, epidermal growth factor-like domain; FNIII, fibronectin type III domain; Ig, immunoglobulin-like domain; LG, laminin G domain; TM, transmembrane domain; VWC, von Willebrand factor type C domain. (B) Interaction between NELL2 and ROBO3 in solid-phase binding assays. Purified Fc-tagged ROBO3-ectodomain (ECD) or three FNIII domains (FNIII) (10 nM) were allowed to bind to protein A-coated plates which were then incubated with purified AP-tagged NELL2 protein (10 nM) at the indicated pH values. The bound AP activity was measured by adding the AP substrate. Each value represents the mean \pm SD of triplicate results. (C) Titration curves of ROBO3-ECD bound to NELL2 at pH 7.4 and 6.5. Purified Fc-ROBO3-ECD protein was allowed to bind to protein A-coated plates at various concentrations which were then incubated with purified AP-tagged NELL2 (10 nM). The bound AP activity was measured as above. (D) Interaction between mouse Nell2 and human ROBO3 in the solution binding assay. Conditioned media containing FLAG-tagged Nell2 and HA-tagged ectodomain (ECD) of ROBO3 were mixed and then incubated with anti-FLAG affinity beads at the indicated pH values. Bound proteins were isolated by immunoprecipitation, resolved by SDS/PAGE, and visualized by immunoblotting with the anti-HA and anti-FLAG antibodies. (E) Interaction between human NELL2 and mouse Robo3 in the cell surface binding assay. COS-1 cells were transiently transfected with an expression plasmid for full-length Robo3 and incubated with conditioned medium containing AP-tagged NELL2 at the indicated pH values. The bound AP was visualized by *in situ* staining with BCIP/NBT. Scale bars, 100 μ m. (F) The interaction between mouse Nell2 and human ROBO3 was measured in biolayer interferometry. The biotinylated ROBO3-ECD (1 μ M) was loaded on a streptavidin chip and incubated with Nell2 at the indicated concentrations and pH values. Association and dissociation were measured for 120 s each. Binding curves are colored black, and the global fit of the data to a 1 : 1 binding model is colored red. Data show representative curves from three technical replicates.

and Glu592 would be strong, possibly making the structure of the NELL2–ROBO3 complex stabilized. Note that no charged amino acids with pK_a shifts around pH 6.5 other than Glu592 were found in the entire EGFL2–3 domain of NELL2 and the FNIII1 domain of ROBO3. The orientation of Asp476–Glu592–Arg630 residues in the previously reported crystal structure of the NELL2–ROBO3 complex (Fig. S2C) [30], which was crystallized at neutral pH, is more similar to our predicted structure at pH 6.0 than that at pH 7.4 (Fig. 2). One potential reason for this discrepancy is that the reported crystal structure

may not accurately reflect the structure at neutral pH because of its crystallization in a buffer with low buffering capacity and data collection under ultra-low-temperature conditions [30].

The Glu592 to Gln592 mutation reduces the binding affinity between NELL2 and ROBO3

To test whether the Glu592 residue is a pH sensor for pH-dependent NELL2–ROBO3 binding, we first performed solid-phase binding assays by replacing Glu592 with Ala592. The results showed that the increase in

Table 1. pK_a predictions for ionizable residues that are located at the NELL2–ROBO3 binding interface using MOE software.

Protein	Residue	Model- pK_a	pK_a		
			pH 8.0 ^a	pH 7.0 ^a	pH 6.0 ^a
NELL2	Arg448	12.50	11.52	11.59	11.38
	His449	6.50	5.03	5.45	7.45
	Arg452	12.50	13.66	13.92	13.52
	Glu453	4.50	−1.63	−1.90	−1.42
	Arg474	12.50	12.42	12.43	11.71
	Asp476	3.80	2.03	2.02	0.87
	Asp477	3.80	2.12	2.27	4.01
	Asp484	3.80	2.62	2.17	2.21
ROBO3	Glu592	4.50	6.81	6.84	10.51
	Arg630	12.50	15.73	15.93	15.55
	Glu639	4.50	0.82	0.83	0.82

^aThe pK_a values of the charged amino acids located at the binding interface were predicted from the NELL2–ROBO3 complex structure with an energy-minimized calculation considering the protonation state at each pH. Model- pK_a values were taken from reference [32].

NELL2 binding affinity at an acidic pH was completely abolished in the E592A mutant of ROBO3-FNIII (Fig. S2D). We next performed solid-phase binding assays by replacing Glu592 with Gln592, which is an isosteric and uncharged change. Again, the results showed that the increase in NELL2 binding affinity at an acidic pH was almost abolished in the E592Q mutant of ROBO3-FNIII (Fig. 3A). Similarly, the increase in NELL2 binding affinity was almost abolished in the E592Q mutant of ROBO3-ECD (Fig. 3B). The titration curve at pH 6.5 using the E592Q mutant of ROBO3-ECD did not exhibit

a concentration-dependent increase in NELL2 binding affinity (Fig. 3C). NELL2–ROBO3 binding has been shown to occur via polar contacts of the FNIII1 domain of ROBO3 to the EGFL2 domain of NELL2, and hydrophobic interaction with the EGFL3 domain of NELL2 (Fig. S2C) [30]. Asp476 of NELL2 and Arg630 of ROBO3 likely form a salt bridge, and each single amino acid substitution mutant prevents the NELL2–ROBO3 binding, suggesting a central role in polar contact between them (Fig. 3D). The Glu592 residue forms a hydrogen bond with both Asp476 and Arg630, “Asp476–Glu592–Arg630 triangle”, in acidic conditions, which may contribute to the increased NELL2–ROBO3 binding affinity. It is likely that Glu592 residue is one of the pH sensors in the pH-dependent NELL2–ROBO3 binding, although the mutation in Glu592 can not only cause loss of protonation but may also affect the conformation in the vicinity.

Because the E592Q mutant of ROBO3 has a charge-neutralizing mutation of the Glu592 residue, there was a possibility that the binding to NELL2 would increase, as in the case of wild-type ROBO3, which is protonated in acidic conditions. However, this did not occur. The following mechanism is assumed to provide an explanation for this. Here, we predicted the structure of the ROBO3-FNIII1 domain alone using AlphaFold3 [33] and found that the Glu639 residue is located near Glu592 and Arg630 residues and they are in a bound state, via ionic interactions (Fig. S3A). However, because of the charge imbalance in the binding among these three residues, either Glu592 or Glu639 is not involved in the interaction and is considered to have side-chain flexibility. In the E592Q

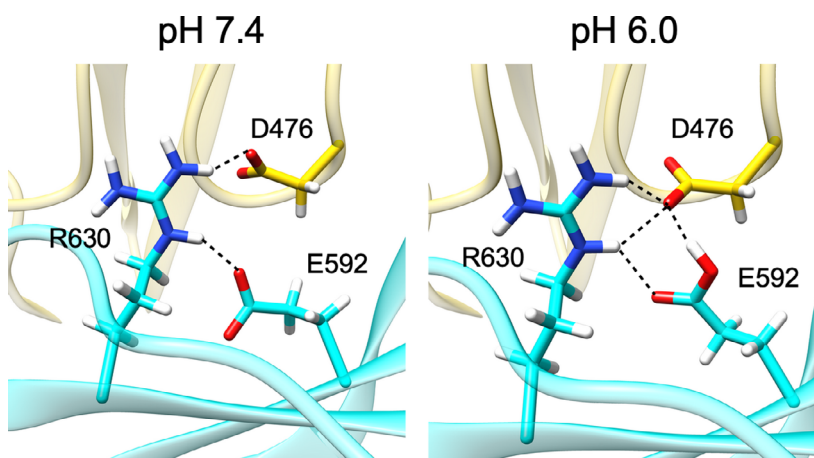


Fig. 2. Estimation of the binding interface structures of NELL2–ROBO3 complex. Structural modeling of NELL2–ROBO3 complex in pH 7.4 (left panel) and pH 6.0 (right panel) based on the crystal structure (PDB ID: 6POG). Ribbon diagrams showing the binding interface between NELL2 (yellow) and ROBO3 (cyan). Key residues are shown as sticks. The Glu592 residue exhibits different protonation states in pH 7.4 and pH 6.0, revealing a rearrangement of the hydrogen bonding network; Glu592 can interact with Asp476 in pH 6.0. Putative hydrogen bonds and salt bridges are shown by dashed lines.

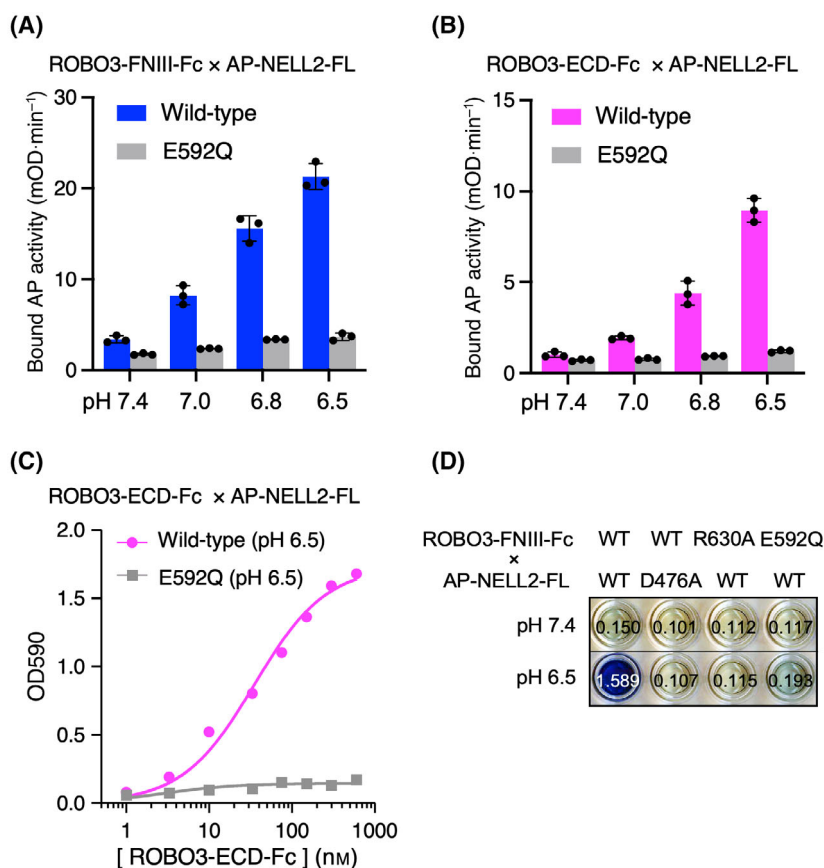


Fig. 3. The Glu592 to Gln592 mutation reduces the binding affinity between NELL2 and ROBO3. (A) Interaction of NELL2 with the human ROBO3-FNIII (wild-type) and its E592Q mutant in solid-phase binding assays. Purified Fc-tagged ROBO3-FNIII and its E592Q mutant (10 nM) were allowed to bind to protein A-coated plates and were then incubated with purified AP-tagged NELL2 protein (10 nM) at the indicated pH values. The bound AP activity was measured by adding the AP substrate. Each value represents the mean \pm SD of triplicate results. (B) Interaction of NELL2 with the ROBO3-ECD (wild-type) and its E592Q mutant in solid-phase binding assays. Purified Fc-tagged ROBO3-ECD and its E592Q mutant (10 nM) were allowed to bind to protein A-coated plates and were then incubated with purified AP-tagged NELL2 protein (10 nM) at the indicated pH values. The bound AP activity was measured as above. (C) Titration curves of ROBO3-ECD (wild-type) and its E592Q mutant bound to NELL2 at pH 6.5. Purified Fc-ROBO3-ECD protein and its E592Q mutant were allowed to bind to protein A-coated plates at various concentrations and were then incubated with purified AP-tagged NELL2 (10 nM). The bound AP activity was measured as above. (D) Results of solid-phase binding assay for the interaction between ROBO3 and NELL2 mutants. Purified Fc-tagged ROBO3-FNIII (WT) and its mutants (R630A and E592Q) (10 nM) were allowed to bind to protein A-coated plates and were then incubated with conditioned media containing AP-tagged NELL2 (WT) or its D476A mutant at the indicated pH values. The amount of conditioned media containing AP-tagged protein was used with equivalent AP activity.

mutant, the interaction between Arg630 and Glu639 residues is predominant, thereby immobilizing the side chain of the Glu639 residue (Fig. S3B). When binding to NELL2, the Glu639 residue faces the Glu453 residue of NELL2, which is thought to cause repulsion due to the negative charge. In wild-type ROBO3, the repulsion between Glu453 and Glu639 residues is relatively weak, allowing NELL2 and ROBO3 to access each other and bind with moderate affinity (Fig. S3C), and the interaction may be stronger under acidic conditions, as described above. In contrast, in the E592Q

mutant, it is assumed that NELL2 is less accessible because of the strong repulsion between the Glu453 and Glu639 residues (Fig. S3D). Therefore, the E592Q mutant is thought to bind poorly to NELL2 at neutral and acidic pH.

Two distinct but related pH-dependent regulatory mechanisms in NELL-ROBO binding

Because the amino acid residues forming the Asp476-Glu592-Arg630 triangle are all conserved in NELL1/2

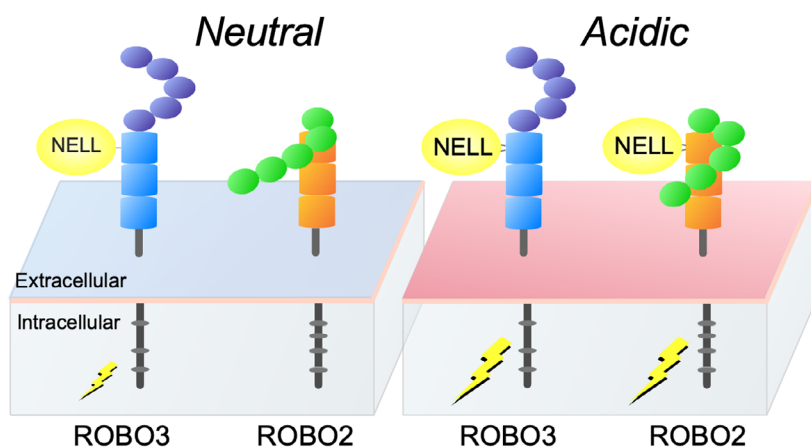


Fig. 4. Summary of a potential pH-dependent interaction between NELL and ROBO2/3. At neutral pH, NELL ligands weakly bind to ROBO3 but not to ROBO2. In acidic conditions, NELL ligands bind strongly to ROBO3 by forming an Asp-Glu-Arg triangle and also bind to ROBO2 by conformational change of ROBO2-ECD. The binding affinity may determine the downstream signal intensity.

and ROBO1–3 amino acid sequences (Fig. S2A), the pH-dependent increase in binding affinity involving protonation of Glu592 may also occur in the NELL1/2–ROBO1/2 combinations. However, ROBO2-ECD must undergo a conformational change process because the FNIII1 domain is masked because of its hairpin-like structure. According to the crystal structure of ROBO2-ECD (PDB ID: 6IAA) [28], Arg596 of ROBO2, which corresponds to Arg630 of ROBO3, forms a hydrogen bond with the main chains of Ile420 and Leu421 in the Ig5 domain (Fig. S4). Thus, maintenance of a hairpin-like structure and NELL binding are in competition for the Arg596 residue. Therefore, in acidic conditions, the conformational change in the hairpin-like structure is thought to occur first [27,29], followed by NELL binding and the formation of the Asp-Glu-Arg triangle. Because ROBO1 is also likely to have a hairpin-like structure [30,34], the process is similar to that in ROBO2. For a correct understanding of NELL–ROBO signaling, a comprehensive analysis of the binding affinity of each ROBO receptor to the NELL ligands at a neutral to acidic pH range is needed.

In *Drosophila*, internalization of the Slit–Robo complex into late endosomes by endocytosis is essential for the downstream signaling [35]. It has also been shown that Slit–Robo1 signaling is regulated by endocytosis in vertebrates [36]. Because the internal environment of early (pH 6.8–5.9) and late (pH 6.0–4.9) endosomes is acidic [37], internalization of the NELL2–ROBO3 complex by endocytosis increases the affinity between NELL2 and ROBO3, but how this affects signal transduction is currently unknown. However, because it has not yet been reported whether ROBO2/3 is internalized by endocytosis [38,39], it is important to determine whether the NELL2–ROBO3 complex functions on the cell surface or is internalized via endocytosis.

In summary, it is possible that NELL–ROBO binding is tightly regulated by pH values because there are two distinct but related pH-dependent control mechanisms for NELL–ROBO binding affinity (Fig. 4). Because the affinity of the NELL2–ROBO3 interaction predominantly determines NELL2 axon repulsive activity [30], these results suggest the existence of a regulatory mechanism of axon guidance by extracellular pH and may provide insight into the physiological significance of pH fluctuations in the brain.

Acknowledgements

We thank Edanz Group (<https://jp.edanz.com/ac>) for editing a draft of this manuscript. This work was supported by the Japan Society for the Promotion of Science (JSPS) KAKENHI Grant Number 20H02948.

Author contributions

KM and TN designed and performed experiments and analyzed data. MT, TO-K, and ADM assisted with data processing. TN wrote the manuscript.

Peer review

The peer review history for this article is available at <https://www.webofscience.com/api/gateway/wos/peer-review/10.1002/1873-3468.15054>.

Data accessibility

The data that support the findings of this study are available from the corresponding author [tniimi@agr.nagoya-u.ac.jp] upon reasonable request.

References

- Chesler M and Kaila K (1992) Modulation of pH by neuronal activity. *Trends Neurosci* **15**, 396–402.
- Chesler M (2003) Regulation and modulation of pH in the brain. *Physiol Rev* **83**, 1183–1221.
- Pavlov I, Kaila K, Kullmann DM and Miles R (2013) Cortical inhibition, pH and cell excitability in epilepsy: what are optimal targets for antiepileptic interventions? *J Physiol* **591**, 765–774.
- Zha XM, Xiong ZG and Simon RP (2022) pH and proton-sensitive receptors in brain ischemia. *J Cereb Blood Flow Metab* **42**, 1349–1363.
- Halim ND, Lipska BK, Hyde TM, Deep-Soboslay A, Saylor EM, Herman MM, Thakar J, Verma A and Kleinman JE (2008) Increased lactate levels and reduced pH in postmortem brains of schizophrenics: medication confounds. *J Neurosci Methods* **169**, 208–213.
- Dogan AE, Yuksel C, Du F, Chouinard VA and Ongur D (2018) Brain lactate and pH in schizophrenia and bipolar disorder: a systematic review of findings from magnetic resonance studies. *Neuropsychopharmacology* **43**, 1681–1690.
- Hagihara H, Catts VS, Katayama Y, Shoji H, Takagi T, Huang FL, Nakao A, Mori Y, Huang KP, Ishii S *et al.* (2018) Decreased brain pH as a shared endophenotype of psychiatric disorders. *Neuropsychopharmacology* **43**, 459–468.
- Pruett BS and Meador-Woodruff JH (2020) Evidence for altered energy metabolism, increased lactate, and decreased pH in schizophrenia brain: a focused review and meta-analysis of human postmortem and magnetic resonance spectroscopy studies. *Schizophr Res* **223**, 29–42.
- Park HJ, Choi I and Leem KH (2021) Decreased brain pH and pathophysiology in schizophrenia. *Int J Mol Sci* **22**, 8358.
- Hagihara H, Shoji H, Hattori S, Sala G, Takamiya Y, Tanaka M, Ihara M, Shibutani M, Hatada I, Hori K *et al.* (2024) Large-scale animal model study uncovers altered brain pH and lactate levels as a transdiagnostic endophenotype of neuropsychiatric disorders involving cognitive impairment. *elife* **12**, RP89376.
- Hagihara H, Murano T and Miyakawa T (2023) The gene expression patterns as surrogate indices of pH in the brain. *Front Psychiatry* **14**, 1151480.
- Dickson BJ (2002) Molecular mechanisms of axon guidance. *Science* **298**, 1959–1964.
- Seiradake E, Jones EY and Klein R (2016) Structural perspectives on axon guidance. *Annu Rev Cell Dev Biol* **32**, 577–608.
- Rozbesky D and Jones EY (2020) Cell guidance ligands, receptors and complexes - orchestrating signalling in time and space. *Curr Opin Struct Biol* **61**, 79–85.
- Klein R and Pasterkamp RJ (2021) Recent advances in inter-cellular interactions during neural circuit assembly. *Curr Opin Neurobiol* **69**, 25–32.
- Dickson BJ and Gilestro GF (2006) Regulation of commissural axon pathfinding by slit and its Robo receptors. *Annu Rev Cell Dev Biol* **22**, 651–675.
- Ypsilanti AR, Zagar Y and Chedotal A (2010) Moving away from the midline: new developments for slit and Robo. *Development* **137**, 1939–1952.
- Blockus H and Chedotal A (2016) Slit-Robo signaling. *Development* **143**, 3037–3044.
- Friocourt F and Chedotal A (2017) The Robo3 receptor, a key player in the development, evolution, and function of commissural systems. *Dev Neurobiol* **77**, 876–890.
- Kaneko N, Herranz-Perez V, Otsuka T, Sano H, Ohno N, Omata T, Nguyen HB, Thai TQ, Nambu A, Kawaguchi Y *et al.* (2018) New neurons use slit-Robo signaling to migrate through the glial meshwork and approach a lesion for functional regeneration. *Sci Adv* **4**, eaav0618.
- Jen JC, Chan WM, Bosley TM, Wan J, Carr JR, Rub U, Shattuck D, Salamon G, Kudo LC, Ou J *et al.* (2004) Mutations in a human ROBO gene disrupt hindbrain axon pathway crossing and morphogenesis. *Science* **304**, 1509–1513.
- Anitha A, Nakamura K, Yamada K, Suda S, Thanseem I, Tsujii M, Iwayama Y, Hattori E, Toyota T, Miyachi T *et al.* (2008) Genetic analyses of roundabout (ROBO) axon guidance receptors in autism. *Am J Med Genet B Neuropsychiatr Genet* **147B**, 1019–1027.
- Lamminmaki S, Massinen S, Nopola-Hemmi J, Kere J and Hari R (2012) Human ROBO1 regulates interaural interaction in auditory pathways. *J Neurosci* **32**, 966–971.
- Blockus H and Chedotal A (2014) The multifaceted roles of slits and Robos in cortical circuits: from proliferation to axon guidance and neurological diseases. *Curr Opin Neurobiol* **27**, 82–88.
- Huang Y, Ma M, Mao X, Pehlivan D, Kanca O, Un-Candan F, Shu L, Akay G, Mitani T, Lu S *et al.* (2022) Novel dominant and recessive variants in human ROBO1 cause distinct neurodevelopmental defects through different mechanisms. *Hum Mol Genet* **31**, 2751–2765.
- Jaworski A, Tom I, Tong RK, Gildea HK, Koch AW, Gonzalez LC and Trssier-Lavigne M (2015) Operational redundancy in axon guidance through the multifunctional receptor Robo3 and its ligand NELL2. *Science* **350**, 961–965.
- Yamamoto N, Kashiwagi M, Ishihara M, Kojima T, Maturana AD, Kuroda S and Niimi T (2019) Robo2 contains a cryptic binding site for neural EGFL-like (NELL) protein 1/2. *J Biol Chem* **294**, 4693–4703.

- 28 Barak R, Yom-Tov G, Guez-Haddad J, Gasri-Plotnitsky L, Maimon R, Cohen-Berkman M, McCarthy AA, Perlson E, Henis-Korenblit S, Isupov MN *et al.* (2019) Structural principles in Robo activation and auto-inhibition. *Cell* **177**, 272–285.e16.
- 29 Miyaguchi M, Nakanishi Y, Maturana AD, Mizutani K and Niimi T (2022) Conformational change of the hairpin-like-structured Robo2 ectodomain allows NELL1/2 binding. *J Mol Biol* **434**, 167777.
- 30 Pak JS, DeLoughery ZJ, Wang J, Acharya N, Park Y, Jaworski A and Ozkan E (2020) NELL2-Robo3 complex structure reveals mechanisms of receptor activation for axon guidance. *Nat Commun* **11**, 1489.
- 31 Pettersen EF, Goddard TD, Huang CC, Couch GS, Greenblatt DM, Meng EC and Ferrin TE (2004) UCSF chimera—a visualization system for exploratory research and analysis. *J Comput Chem* **25**, 1605–1612.
- 32 Li H, Robertson AD and Jensen JH (2005) Very fast empirical prediction and rationalization of protein pKa values. *Proteins* **61**, 704–721.
- 33 Abramson J, Adler J, Dunger J, Evans R, Green T, Pritzel A, Ronneberger O, Willmore L, Ballard AJ, Bambrick J *et al.* (2024) Accurate structure prediction of biomolecular interactions with AlphaFold 3. *Nature* **630**, 493–500.
- 34 Aleksandrova N, Gutsche I, Kandiah E, Avilov SV, Petoukhov MV, Seiradake E and McCarthy AA (2018) Robo1 forms a compact dimer-of-dimers assembly. *Structure* **26**, 320–328.e4.
- 35 Chance RK and Bashaw GJ (2015) Slit-dependent endocytic trafficking of the Robo receptor is required for son of Sevenless recruitment and midline axon repulsion. *PLoS Genet* **11**, e1005402.
- 36 Kinoshita-Kawada M, Hasegawa H, Hongu T, Yanagi S, Kanaho Y, Masai I, Mishima T, Chen X, Tsuboi Y, Rao Y *et al.* (2019) A crucial role for Arf6 in the response of commissural axons to slit. *Development* **146**, dev172106.
- 37 Huotari J and Helenius A (2011) Endosome maturation. *EMBO J* **30**, 3481–3500.
- 38 Bisiak F and McCarthy AA (2019) Structure and function of roundabout receptors. *Subcell Biochem* **93**, 291–319.
- 39 Sullivan KG and Bashaw GJ (2023) Intracellular trafficking mechanisms that regulate repulsive axon guidance. *Neuroscience* **508**, 123–136.

Supporting information

Additional supporting information may be found online in the Supporting Information section at the end of the article.

Fig. S1. Preparation of fusion proteins used in this study.

Fig. S2. Mutational analysis and structural features of NELL2–ROBO3 complex.

Fig. S3. Putative mechanisms of interaction between NELL2 and ROBO3-E592Q mutant.

Fig. S4. Structural features of human ROBO2 ectodomain.

Table S1. The equilibrium dissociation constant (K_D) and kinetic constants (k_a and k_d).